HHS Public Access

Author manuscript

Cell Rep. Author manuscript; available in PMC 2017 July 12.

Published in final edited form as:

Cell Rep. 2016 November 01; 17(6): 1699–1710. doi:10.1016/j.celrep.2016.10.010.

In vivo interrogation of spinal mechanosensory circuits

Amelia J. Christensen[*,1], **Shrivats M. Iyer**[*,2], **Amaury François**[3,4], **Saurabh Vyas**[2], **Charu Ramakrishnan**[2], **Sam Vesuna**[2], **Karl Deisseroth**[2,5,6], **Grégory Scherrer**[†,3,4,7,8], and **Scott L. Delp**[†,‡,2,9]

[1]Department of Electrical Engineering, 318 Campus Drive, Stanford University, Stanford, CA 94305, USA

[2]Department of Bioengineering, 318 Campus Drive, Stanford University, Stanford, CA 94305, USA

[3]Department of Anesthesiology, Perioperative and Pain Medicine, 318 Campus Drive, Stanford University, Stanford, CA 94305, USA

[4]Department of Molecular and Cellular Physiology, 318 Campus Drive, Stanford University, Stanford, CA 94305, USA

[5]Department of Psychiatry and Behavioral Sciences, 318 Campus Drive, Stanford University, Stanford, CA 94305, USA

[6]Department of Howard Hughes Medical Institute, 318 Campus Drive, Stanford University, Stanford, CA 94305, USA

[7]Department of Neurosurgery, 318 Campus Drive, Stanford University, Stanford, CA 94305, USA

[8]Department of Stanford Neurosciences Institute, 318 Campus Drive, Stanford University, Stanford, CA 94305, USA

[9]Department of Mechanical Engineering, 318 Campus Drive, Stanford University, Stanford, CA 94305, USA

Summary

Spinal dorsal horn circuits receive, process, and transmit somatosensory information. To understand how specific components of these circuits contribute to behavior, it is critical to be able to directly modulate their activity in unanesthetized *in vivo* conditions. Here, we develop

Corresponding authors: Scott L. Delp; James H. Clark Center S321, 318 Campus Drive, Stanford, CA 94305, delp@stanford.edu, 650-723-1230. Grégory Scherrer; 1050 Arastradero Road, Building A - Room A151, Palo Alto, California 94304, gs25@stanford.edu.
*These authors contributed equally to this work.
†Co-corresponding authors
‡Lead contact.

Author Contributions

A.J.C, S.M.I., G.S. and S.L.D. designed the experiments. A.J.C, S.M.I., and S. Vyas performed experiments. A.F. performed electrophysiology. S. Vesuna performed histology. C.R. cloned vectors. K.D. contributed reagents and tools. K.D., G.S., and S.L.D. supervised students. A.J.C., S.M.I., G.S., and S.L.D. wrote and edited the paper, with comments from all other authors.

experimental tools that enable optogenetic control of spinal circuitry in freely moving mice using commonly available materials. We use these tools to examine mechanosensory processing in the spinal cord, and observe that optogenetic activation of somatostatin+ interneurons facilitates both mechanosensory and itch-related behavior, while reversible chemogenetic inhibition of these neurons suppresses mechanosensation. These results extend recent findings regarding processing of mechanosensory information in the spinal cord and indicate the potential for activity-induced release of the somatostatin neuropeptide to affect processing of itch. The spinal implant approach we describe here is likely to enable a wide range of studies to elucidate spinal circuits underlying pain, touch, itch, and movement.

Graphical abstract

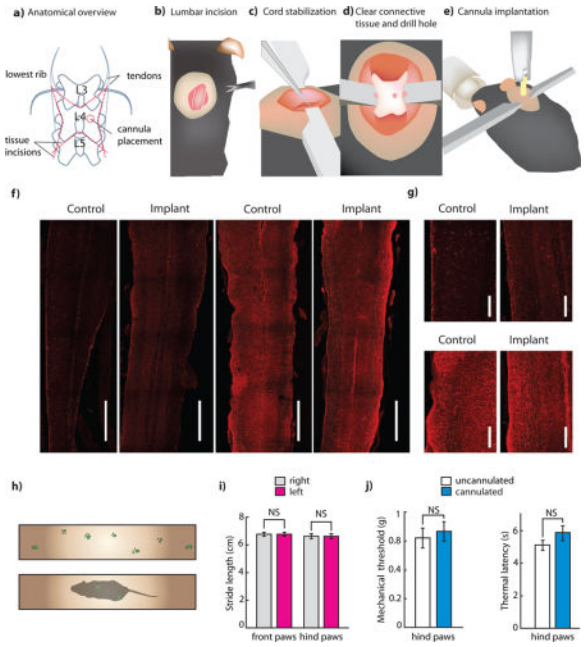

Introduction

A key virtue of the optogenetic approach to the control of neural circuitry has been the ability to directly link neural activation to behavior, and in so doing, test predictions of proposed circuit models. While this approach has been very powerful in the brain (Adamantidis et al., 2015; Boyden, 2015; Deisseroth, 2015), and peripheral nervous system (Copits et al., 2016; Iyer et al., 2014; Montgomery et al., 2016), the application of optogenetic control in the mammalian spinal cord has been largely restricted to *ex vivo* slice preparations (Carr and Zachariou, 2014; Dougherty et al., 2013; Foster et al., 2015; Hägglund et al., 2013, 2010; Talpalar et al., 2011; Wang and Zylka, 2009; Yang et al., 2015; Zhang et al., 2014), which do not allow for direct analysis of the behavioral consequences of neural control.

One of the most influential circuit models in the spinal cord is the ‘gate control circuit’, proposed by Melzack and Wall in 1965 (Melzack and Wall, 1965) to explain empirical

observations related to acute and chronic pain perception, specifically, the emergence of allodynia in chronic pain, and the dampening of pain sensation by innocuous touch. In this model, light touch fibers preferentially synapse on an inhibitory interneuron (a 'gate' cell) in the dorsal spinal cord, but also synapse on an excitatory projection neuron (known as a 'T' cell). Pain fibers synapse only on the 'T' cell, which also receives inhibitory drive from the 'gate' cell. Thus in non-pathological conditions, light touch acts to dampen pain sensation, through activation of the 'gate' cell. This is in contrast to chronic pain conditions, wherein the 'gate' cell inhibition efficacy reduces, and thus the activation of light touch fibers induces, instead of attenuates, pain. Fifty years after the proposal of this circuit, neurons whose electrophysiological response properties agree with major testable predictions of this model have been identified. Specifically in mechanosensation, somatostatin+ interneurons, glutamatergic neurons in layer 2/3 of the superficial dorsal horn, have been proposed as the 'T' cell in the Melzack and Wall model (Duan et al., 2014). While behavioral responses to ablation of these neurons, i.e. a reduction in mechanical sensitivity and mechanical allodynia, agree with Melzack and Wall's predictions (Duan et al., 2014), researchers have lacked the tools to test predictions associated with the activation of these neurons *in vivo*.

Here, we developed a method to optogenetically activate dorsal horn neurons in awake, behaving rodents that was compatible with typical pain assays, and relied only on off-the-shelf products. Using this system, we find that activation of somatostatin+ neurons results in strong nocifensive behavior in an array of pain assays, in broad agreement with gate control model predictions. We also report that this neural population plays a role in regulating pruritoception, most likely through activity-dependent release of the neuropeptide somatostatin. While these results indicate that activation of somatostatin+ neurons is generally consistent with predictions from the gate control model, they also suggest that this population of neurons may play a broader role in the regulation and processing of peripheral somatosensory signals, highlighting the complex and interwoven nature of spinal circuitry.

Results

Implantation strategy and characterization of *in vivo* utility

We first developed a surgical implantation procedure to attach a standard fiber optic ferrule (commonly used in the brain) to the thoracic or lumbar spinal column (Figure 1a; Figure S1; see Supplementary Surgical Protocol). Two primary constraints guided procedure development. First, the implant should be secured to only a single vertebral segment to allow for free movement of the spinal column (Figures 1b–c). Second, the implant should not penetrate the spinal parenchyma, but instead must remain superficial to the cord, due to the relative motion between the cord and its vertebral housing (Figures 1d–e).

After cannula implantation, mice remained housed in a group, and displayed no visible signs of distress or pathology. To assess this, we quantified mouse behavior in affective, motor, and somatosensory tasks, and observed no implantation related deficits (Figures 1h–k, Figure S2). To verify cannula placement, we performed *in vivo* anesthetized recordings from the spinal cord segment in which we implanted our cannula (lumbar segment 4), and confirmed that dorsal horn neurons in that region had a receptive field on the plantar surface of the ipsilateral hind-paw (Figure S2).

As a proxy for implant-induced damage, we stained sections from implanted mice for markers for microglia (Iba1) or astrocytes (GFAP) (Figure 1f,g) (Canales et al., 2015). We compared these sections to those from control mice that had received a sham surgery, but did not have a cannula implanted, and observed no difference between sections from the two sets of mice. We performed this characterization approximately 14 days after cannula implantation, the time point at which we generally began our behavioral experiments. Of the over 150 cannulations we have performed since developing the procedure, cannulae have become dislodged prior to the sacrifice of the animal in only 6 cases, comparable to the failure rates observed in standard brain cannula implantation procedures.

To verify that we could drive behavioral changes by optogenetically activating neurons in the spinal cord with light delivered through our implanted cannula we expressed ChR2 in a nonspecific population of spinal cord neurons through intraparenchymal injection of AAVDJ:CaMKIIa:ChR2-eYFP in the spinal cord. The transduced population included dorsal and ventral horn neurons, such that optical activation caused visible hind limb contraction and nocifensive behavior (Figure S2, Supplementary Video 1). We histologically verified optical activation of neurons through staining for c-Fos (Figure S2). In addition to verifying that light delivered through implanted cannulae could drive behavioral responses, these results also demonstrated potential applications of this technique to studying ventral horn circuits underlying spinal motor control. We performed a Monte Carlo simulation of light propagation (Stujenske et al., 2015) to determine the expected depth of functional optogenetic excitation (Fig. S2). We observed that sufficiently high levels of light intensity (>0.5 mW/mm^2) could be achieved at depths up to 1 mm in the spinal cord with 10 mW of light output from the fiber.

Optogenetic activation of somatostatin+ interneurons

Having validated the utility of the spinal cord implant for *in vivo* neuromodulation, we then turned to the gate control circuit model. If somatostatin+ interneurons are homologous to ‘T’ cells, the model (Figure 2a) predicts that their activation would directly engage ascending pain pathways. This would be reflected behaviorally both through an immediate reflexive nocifensive response, as well as through behavioral manifestations of aversion representing the affective dimension of pain (associated negative emotional valence) (Duan et al., 2014; Melzack and Wall, 1965).

To test this prediction, we injected transgenic mice expressing Cre in somatostatin neurons (SOM-Cre mice) with AAV:Ef1a:DIO:ChR2-eYFP. The extent and distribution of ChR2-eYFP expression was largely as previously described (Duan et al., 2014), with an enrichment of cell bodies dorsal to, but not overlapping with, PKCγ neurons (which denote the lamina II/III border (Malmberg et al., 1997), and a dense network of axons and dendrites throughout the dorsal horn (Figure 2b). Importantly, we saw no retrograde expression of ChR2-eYFP in DRG neurons (Figure 2b).

We verified with slice electrophysiology that blue light illumination of SOM-ChR2 neurons evoked light-induced current and subsequent action potentials at intensities as low as 0.002 mW/mm^2 (Fig. S3). Light-evoked current increased with increasing light power density, as did the probability of action potential generation. ChR2 expressing neurons faithfully

followed light pulse trains with frequency ranging from 1 to 10 Hz (10 ms pulse width). Consistent with known properties of ChR2, probability of action potential generation decreased at higher frequencies (Supplementary Figure 2).

Next, we optogenetically stimulated SOM-ChR2 interneurons in awake mice. Consistent with model predictions, mice showed an immediate nocifensive response to blue light stimulation (Figure 2c, Supplementary Video 2). Mice consistently licked the appropriate dermatomes, and with variation in lumbar implant site engaged in licking that ranged in location from the ipsilateral thigh to the plantar surface of the ipsilateral hind paw. We then assessed whether a negative emotional valence was associated with activation of somatostatin+ neurons, by testing whether optogenetic activation was sufficient to generate conditioned place aversion (Figures 2g). We found SOM-ChR2 mice spent significantly less time in the chamber in which light was delivered after a training period, while control mice expressing YFP did not show any preference.

We then determined the light level that would elicit a behavioral response from each mouse. This level ranged from 40 μW to 3 mW, and was less than 0.5 mW in 4 out of 6 tested mice. Higher intensity thresholds are likely due to obstruction of the cannula-spinal cord interface (Figure 2d, S2m). We used each mouse's individual 'threshold' to determine light levels for future behavioral experiments. We tested whether blue light stimulation below this threshold would change the response of the mice to mechanical and thermal stimuli. If somatostatin+ neurons form the output of a purely mechanosensory gait circuit, then sub-threshold activation of these neurons would decrease mechanical, but not thermal thresholds. Consistent with these predictions, we found that sub-threshold activation of somatostatin interneurons significantly reduced mechanical thresholds on the von Frey test, but did not alter thermal thresholds on the Hargreaves test (Figures 2e–f).

Transient inhibition of somatostatin+ interneurons

Previous studies examining somatostatin+ interneurons have used genetic ablation strategies to characterize the function of these neurons. However, recent reports indicate that the results of transient neural silencing may differ dramatically from the results of permanent ablation (Otchy et al., 2015). We therefore tested whether transient inhibition of somatostatin+ interneuron activity would confirm model predictions, recapitulating aspects of previously observed behavior (Duan et al., 2014). Two major strategies have been used to reversibly inhibit neural circuits—optogenetic inhibition (Adamantidis et al., 2015; Boyden, 2015; Deisseroth, 2015) and the use of chemogenetic Gi-coupled DREADDs (Armbruster et al., 2007; English and Roth, 2015; Iyer et al., 2016; Urban and Roth, 2015). Here, we adopted a chemogenetic strategy for two reasons: 1) lamina II neurons exhibit large rostro-caudal patterns of activation in response to primary afferent input (Nishida et al., 2014), and we were concerned that the narrow field of illumination provided by an implanted fiber optic ferrule would not be sufficient to drive behavior and 2) optogenetic inhibition typically requires high intensity constant light, which, given the high density of TRPV1 expression in nociceptor terminals in the dorsal spinal cord, poses a significant heating-related activation confound.

We injected SOM-Cre mice intraspinally with AAV5:hSyn:DIO:hM4D(Gi)-mCherry, and assessed nociception with mechanical and thermal assays. hM4D(Gi)-mCherry expression was consistent with previous results (Figure 2h, Figure S4a). If SOM+ neurons are the 'T-cells' in the gate control model, then they should relay input from Aδ and C-HTMR primary afferents to ascending pain pathways. Therefore, chemogenetic inhibition of these neurons would be predicted to transiently increase mechanical withdrawal thresholds. Gate control also predicts that in naïve animals, input from light-touch afferents (Aβ-, Aδ- and C-LTMRs) should not be sufficient to drive activation of 'T-cells', and therefore chemogenetic inhibition of SOM+ cells should not have any effect on light touch. However, in mice exhibiting mechanical allodynia, input from light-touch afferents is relayed through 'T-cells', and therefore chemogenetic inhibition of SOM+ cells should meaningfully reduce mechanical hypersensitivity. Our behavioral results were consistent with these predictions. In naïve SOM-hM4Di mice we observed that following intraperitoneal injections of clozapine-N-oxide (CNO), but not saline, mice showed a significant increase in mechanical withdrawal thresholds, as well as a slight increase in heat withdrawal latency, but no reduction in sensitivity to a measure of light touch (cotton swab assay, Figures 2 i–k). To examine the effects of chemogenetic inhibition on mechanical allodynia, we injected the paws of the animals with Complete Freund's Adjuvant (CFA), a pro-inflammatory agent. As expected, CFA injection caused dynamic mechanical allodynia (Figure 2k). Consistent with model predictions, intraperitoneal injection of CNO now significantly reduced allodynia, restoring light-touch sensitivity to baseline pre-CFA levels (Figure 2k). In addition, mice expressing hM4Di displayed no differences in measures of locomotion following CNO administration, as compared with following saline injection, suggesting these results are not due to motor related confounds (Figure S4b).

Temporally sparse optogenetic stimulation of somatostatin+ interneurons increases histamine-induced itch

In recent work, it has been demonstrated that intrathecal administration of the somatostatin analog octreotide results in strong scratching behavior that can be eliminated by ablation of Bhlhb5 neurons, which are a subpopulation of neurons that express the 2A isoform of the somatostatin receptor (SST2AR) (Kardon et al., 2014). When we immunostained spinal cord sections from mice expressing ChR2 in somatostatin+ neurons for SST2AR, we noticed significant spatial overlap between regions of strong ChR2-eYFP expression, and regions of strong SST2AR expression (Figure 3a). Thus, we were curious if, in addition to their role in gate control, somatostatin+ neurons may contribute to regulation of itch, through activity-dependent release of somatostatin. We designed an experiment to test this hypothesis. We injected histamine intradermally into the thigh of somatostatin+ mice expressing either ChR2 or mCherry, and concurrently performed intrathecal (IT) injections of either saline or the SST2R antagonist CYN-154806. We then optogenetically stimulated these mice with a temporally sparse 1 Hz, 100 ms pulse train, titrating light intensity on a mouse-by-mouse basis to minimize stimulation evoked paw-licking behavior, and then video recorded histamine-evoked thigh-biting behavior. We observed that in SOM-ChR2 mice, but not in SOM-mCherry controls, optogenetic stimulation paired with IT saline resulted in high rates of histamine-evoked thigh biting, as compared to optogenetic stimulation paired with IT CYN-154806 (Figure 3b). In contrast, when temporally sparse optogenetic stimulation and

IT saline/CYN-154806 were paired with measures of mechanical and thermal sensitivity, no significant differences were observed upon optogenetic stimulation in either IT saline, or IT CYN-154806 conditions (Figures 3c–d).

Somatostatin+ neuron activation recruits ascending pain pathways

A critical prediction of gate theory is that activation of 'T-cells' results in recruitment of ascending pain pathways. Although previous work (Duan et al., 2014) suggested that somatostatin+ interneurons relay mechanosensory information to neurons in laminae I and II, the genetic identity of these neurons, and whether they project to supraspinal centers, was unknown. We assayed downstream activity induced by optogenetic activation of SOM+ neurons through c-Fos immunohistochemistry. We found c-Fos+ neurons in both superficial laminae and deep dorsal horn laminae, including neurons that express NK1R, a subset of which are known to relay pain information to supraspinal centers (Todd, 2002) (Figures 4 a–h).

Discussion

In the past decade, researchers have begun to employ increasingly sophisticated *in vivo* genetic tools to piece together subsets of spinal cord sensory circuits responsible for processing external stimuli. These tools have enabled the investigation of behavioral responses to ablation of subsets of dorsal horn neurons, either during development (Duan et al., 2014), or in adulthood (Foster et al., 2015). However, these approaches are not without limitations: genetic knock out strategies can introduce interpretational confounds due to the absence of knocked out genes during development, while cellular ablation is permanent and may differ in its effects from transient silencing (both due to the potentially toxic by-products of cellular ablation, and recently characterized differences between the effects of transient and chronic neural silencing (Otchy et al., 2015)).

Here, we have described how standard optogenetic tools can be co-opted for use in the spinal cord, enabling direct selective control of spinal circuits in freely moving mice. The implantation strategy we describe does not impede locomotion, alter baseline responses to measures of somatosensory sensitivity, or induce significant anxiety. The optogenetic tools we use in this work are currently available for ~$20 per implant, and require no additional fabrication or construction after purchase. They therefore may enable a substantial cost and time-saving for the large fraction of experiments in which wirelessly powered implants (Ho et al., 2015; Montgomery et al., 2015; Park et al., 2015) are unnecessary. A recent publication by Bonin et al., 2016 describes an alternative tethered approach to light-delivery to the spinal cord in which the fiber optic cable is attached to the skull, and tunneled epidurally until it rests dorsal to the cord (Bonin et al., 2016). This approach is valuable in experiments where stimulation and injection of a large rostro-caudal section of the spinal cord is useful; however, as the emitted light from such implants spreads spherically, only a quarter of the emitted light is directly ventrally into the cord, reducing the maximum light intensity that can be achieved using this approach.

In addition to controlling sensory dorsal horn circuits, the optogenetic implantation procedure described here could be applied to dissect a variety of physiological processes

controlled by spinal circuitry. These include locomotion and respiration-related motor circuits, which have been studied extensively in ex vivo (Dougherty et al., 2013; Hägglund et al., 2013, 2010) and anesthetized preparations (Alilain et al., 2008; Wang et al., 2013) but which have not been manipulated in freely moving unanesthetized animals.

These results form part of a growing body of knowledge regarding the molecular identity and functional role of the neurons that comprise the gate control circuit in the spinal dorsal horn (Bourane et al., 2015; Duan et al., 2014; Petitjean et al., 2015). In particular, the rapid and strong nature of the behavioral response to SOM-ChR2 stimulation was striking. Mice engaged in highly consistent patterns of examining and licking the dermatomally appropriate region, but did not typically shake their paw or flinch (as we have previously observed in response to optogenetic activation of ummyelinated primary afferent nociceptors, or as is observed in the von Frey or Hargreaves test). This response highlights the strong salience of somatostatin+ neuron activation, and is consistent with the pattern of activity-induced c-Fos, and predictions from the gate control model.

Our results demonstrating the consequences of transiently chemogenetically suppressing somatostatin+ interneurons broadly agree with previous ablation studies (Duan et al., 2014). This is particularly interesting given that the neuronal population we controlled (both during optogenetic activation and during chemogenetic inhibition) is restricted to neurons that express somatostatin in adulthood. Unlike previous reports that used a developmental genetic intersectional strategy (Duan et al., 2014), we do not observe overlap of transgene expression with the PKCγ neuronal population, indicating that inhibition of the SOM+ PKCγ− population is sufficient to drive gate control theory-predicted inhibition of mechanical allodynia.

Our results here synthesize two lines of evidence regarding processing of mechanosensation and pruritoception in the spinal cord (Duan et al., 2014; Kardon et al., 2014). Optogenetic activation of somatostatin+ interneurons results in an increase in histamine-evoked itch behavior that may be mediated through the somatostatin neuropeptide, and therefore through suppression of SST2AR expressing neurons, indicating a broader role for these neurons in the regulation of somatosensory stimuli beyond their excitatory role in gating mechanosensory inputs. It remains to be seen whether endogenous activity in somatostatin+ neurons can result in somatostatin release, and if so, how such release interacts with the inhibition of itch by counter-stimuli (Snyder and Ross, 2015). In addition to a somatostatin-mediated effect on itch, it is important to note that our experiments do not rule out a potential additional glutamatergic effect. Future experiments will be required to more completely assess the relative contribution of these two pathways to itch perception. However, the attenuation of optogenetically-evoked itch facilitation by intrathecal administration of SST2R antagonists indicates that somatostatin plays a significant role in this process. These results are indicative of the broader palette of experiments now possible due to easy optogenetic access to the spinal dorsal horn.

Experimental Procedures

Animal test subjects and experiments

Animal procedures were approved by the Stanford University Administrative Panel on Laboratory Animal Care. Mice were either female C57BL/6 mice or Ssttm2.1(cre)Zjh/J mice (Jax 013044), and housed under a 12:12 light/dark cycle, with food and water available *ad libitum*. Mice were randomly assigned by cage to control and experimental groups, and controls and experimental groups were age matched. For all experiments, mice were 6–10 weeks old at the time of injection/implantation, and received cannula implantation approximately 2 weeks prior to beginning of experiments. Control mice for optogenetic somatostatin experiments were C57BL/6 mice (the genetic background of the SOM transgenic mice) and received spinal cord injections of AAVDJ:CaMKIIa:eYFP.

General statistical methods

Data that were known to be drawn from a non-normal distribution (von Frey measures of mechanical withdrawal) were analyzed using non-parametric statistical tests such as the Mann-Whitney U. In some cases (spontaneous response score) the data were transformed such that it was normal, and then a two-way ANOVA was used to detect significance. All data were analyzed using paired tests; generally, the two-tailed Student's *t*-test was used, except for comparing group percentage changes in conditioned place aversion. In that case, as the populations had similar variance, a homoscedastic test, such as Levene's test, was used. Finally, sample sizes were estimated using $\alpha = 0.05$ and power $(1 - \beta) = 0.8$. Based on prior pilot experiments, effect sizes of 0.5–0.8 resulted in sample sizes of approximately 5–10 mice for the behavioral experiments.

Inclusion/Exclusion criteria

Exclusion conditions were determined prior to the beginning of experiments. For all experiments, prior to blinding, mice were tested for sensitivity to light. Mice who did not display a response upon illumination were excluded from study. Under this condition, one mouse was excluded from the AAVDJ:CaMKIIa:ChR2-eYFP experiments. All SOM-ChR2 mice were light sensitive on initial testing. Mice were also excluded if their cannulae became dislodged during experiments. 1 SOM-ChR2 mice was excluded under this criteria. For CPP tests, if on initial testing mice showed a preference for a specific side of the chamber that was greater than 65% or less than 35% they were excluded. One SOM-ChR2 mouse was excluded under these criteria.

Spinal cord injection and implantation of fiber optic cannulae

Virus Preparation—For initial behavioral characterization experiments 6–8 week old C57BL/6 female mice (Charles River) were injected with 2 μl AAVDJ:CaMKIIa:ChR2-eYFP (2×10^{12} vg/ml) or 2 μl AAVDJ:CaMKIIa:eYFP (3.4×10^{2} vg/ml). For somatostatin experiments, 6–8 week old SOM-Cre mice were injected with 1 to 2 μl AAVDJ:ef1a:DIO:ChR2-eYFP (2×10^{12} vg/ml), or 6–8 week old C57BL/6 mice were injected with 1 to 2 μl AAVDJ:CaMKIIa:eYFP (3.4×10^{12} vg/ml). For chemogenetic

experiments, 6–8 week old SOM-Cre mice were injected with 1μl AAVDJ:ef1a:DIO:HM4D(Gi)-mCherry, or AAV5:ef1a:DIO-mCherry.

Injection and Implantation—Spinal cord injections and implantations are described in detail in the supplementary protocol. Briefly, mice were anesthetized under 2–3% isoflurane. Once a stable plane of anesthesia was reached, the area surrounding the dorsal hump was shaved, and then cleansed with alternating applications of betadine and alcohol. A 1–2 cm incision was made slightly caudal to the peak of the dorsal hump in order to expose the lumbar spinal region. The vertebra of interest was identified, and then a small incision was made between the tendons and the vertebral column on either side. The vertebra was then secured using spinal adapter clamps, and all the tissue was removed from the surface of the bone. Using a micro drill, we removed the spinous process, and roughed the surface of the vertebra. Next a small hole was drilled about 2 mm from midline, centrally on the rostral caudal axis. If injections were necessary, they were made through this hole at a depth of approximately 200 μm from the surface of the spinal cord, using standard stereotaxic injection procedures. 1–2 μl of virus was injected at a rate of 0.15 μl/min. We waited 5–10 minutes before removing the needle.

If a cannula was to be implanted, we first cleaved the end of the fiber optic to a length less than 1 mm, and then positioned it above the drilled hole. We used a small amount of super glue around the drill hole and over the surface of the bone, to reduce the possibility of bone bleeds, and to secure the cannula in place. Next we dental cemented the cannula in place, and then after the dental cement dried, sutured the skin surrounding the dental cement. We gave carprofen and buprenorphine subcutaneously, and lidocaine locally. Mice were allowed to recover under a heat lamp before being returned to their cage. Mice continued to be group housed after this procedure was performed.

Conditioned place aversion

Conditioned place aversion experiments were performed largely as previously described (Cunningham et al., 2006). On the first day of testing, mice were first contained to the central room for 1 minute, and then allowed to freely roam the apparatus for 30 minutes. On the 2nd through 4th days mice were contained to the non-stimulation side of the chamber for 10 minutes in the morning, and then at least 4 hours later, they were contained to the opposite side of the chamber for another 10 minutes, where they received optogenetic stimulation. Control and experimental mice were randomly assigned to sides of the chamber, such that the number receiving stimulation in each side was balanced. For somatostatin mice, stimulation parameters were 10 Hz blue light at a 20% DC, at a stimulation intensity 130–150% of the previously determined threshold value. Control mice were randomly assigned stimulation intensity such that each control mouse had the same stimulus parameters as one of the experimental mice. The same number of control and experimental mice were tested, thus the stimulation parameters were exactly matched between groups.

Electrophysiology

In vivo electrophysiology was performed largely as previously described (Yizhar et al., 2011). In brief, a laminectomy was performed on the L4 vertebra segment, and an optrode

was lowered as superficially into the spinal cord as possible. Units were located by listening to their firing while the optrode was advanced or retracted until the point at which maximum amplitude of firing was obtained. To screen for receptive fields, forceps were lightly tapped against the skin until an area that the unit responded to was found. Units for whom a receptive field could not be found were not included in this study. Units were classified based on whether their receptive field was on the plantar surface of the right hind paw or not, and the *xyz* coordinates of the unit were recorded using a digital stereotaxic display. 0 was considered the intersection of the L3 and L4 spinal vertebral segments, at midline.

Spinal cord slice preparation and electrophysiology

Spinal cord slice preparation and electrophysiology were performed as has been previously described (Bardoni et al., 2014). Briefly, two weeks after virus injections, mice were anesthetized with isoflurane, decapitated and the vertebral column was rapidly removed and placed in oxygenated ice-cold dissection solution (in mM: 95 NaCl, 2.5 KCl, 1.25 NaH_2PO_4, 26 $NaHCO_3$, 50 sucrose, 25 glucose, 6 $MgCl_2$, 1.5 $CaCl_2$, and 1 kynurenic acid, pH 7.4, 320 mOsm). The lumbar spinal cord was isolated, embedded in a 3% agarose block and transverse slices (400 μm thick) were made using a vibrating microtome (Leica VT1200). Slices were incubated in oxygenated recovery solution (in mM: 125 NaCl, 2.5 KCl, 1.25 NaH_2PO_4, 26 $NaHCO_3$, 25 glucose, 6 $MgCl_2$, and 1.5 $CaCl_2$, pH 7.4, 320 mOsm) at 35° C for 1 hour. Patch-clamp recording in whole-cell configuration was performed at room temperature on lamina II neurons visualized with an Olympus BX51WI with Nomarski optics and connected to a camera (Q-imaging). Recordings were performed in current-clamp mode or voltage-clamp mode at a holding potential of −70 mV. Thick-walled borosilicate pipettes, having a resistance of 3–5 MOhm, were filled with internal solution (in mM: 120 K-methyl-sulfonate, 10 NaCl, 10 EGTA, 1 CaCl2, 10 Hepes, 0.5 NaGTP, 5 MgATP, pH adjusted to 7.2 with KOH, osmolarity adjusted to 305 with sucrose). Light stimulations were evoked via Lambda Tled controller at a wavelength of 530 nm (Sutter). Data were acquired using a Multiclamp 700A amplifier and pClamp9 software (Molecular Devices, USA). Sampling rate was 10 kHz and data were filtered at 2 kHz.

Measurement of threshold light intensity

To measure the ‘threshold’ light intensity at which somatostatin mice began responding to stimulation, mice were placed in individual tubes with cannulae attached and allowed to first habituate for 30 minutes. Following habituation, each mouse was sequentially screened for approximate current driving a Thorlabs LED driver at which they flinched. Once an approximate current was established, testing began 30–40 mA below that threshold. A stopwatch was used to measure the latency until mice attended the stimulus (which was a lick response in all cases). A cutoff value of 20 s was chosen (i.e. stimulus did not continue more than 20 seconds). At 5 minute intervals, LED intensity was increased by 10 mA. Once the time to attendance dropped below 1 second, tests were halted. The current value at which the mouse response time first dropped below 20 s was chosen as the ‘threshold’ value, and was used in future experiments with that specific mouse. These current values were then normalized to ‘threshold’, and plotted against threshold plus or minus a delta (10 mA steps).

Measurement of mechanical withdrawal thresholds

Mice were habituated to the testing apparatus for 30 minutes prior to testing. Von Frey hairs of different forces were applied to the plantar surface of the paw using a previously described up-down method (Chaplan et al., 1994). The following counted as withdrawal responses: rapid flinch or withdrawal, paw flutter, spreading of the toes or licking of the paw.

For measurements comparing cannulated mice with wild type mice, an opaque sheet of construction paper was wrapped around the containment tube, such that only the paws of the mice were visible to the experimenter. This allowed experimenters to be blinded to the condition of the mice.

For measurements of mechanical withdrawal threshold during sub threshold blue light illumination, mice were assigned an individual light power based on previous experiments. A value of 80% of 'threshold' was assigned to each mouse, as well as a randomly assigned control partner mouse. Stimulation was always 10 Hz at 20% duty cycle. During the test, a second unblinded experimenter adjusted the threshold from mouse to mouse, without revealing the light power to the experimenter performing the test. Different light output powers were not visually distinguishable.

Measurement of thermal withdrawal latency

We measured thermal sensitivity using a Hargreaves apparatus (Ugo Basile). For experiments comparing wild type mice with cannulated mice, the containment tubes were wrapped with construction paper as in the von Frey test. Sub threshold blue light experiments were performed using the same experimental paradigm as used in the von Frey test.

Chemogenetic experiments

Compound administration—In all chemogenetic experiments, the ligand used was clozapine-N-oxide (CNO, C0832, Sigma-Aldrich). CNO was diluted to a concentration of 2 mg/ml in phosphate-buffered saline (PBS) and administered to the animal in a 100 μl dose for a dose of 200 μg (~10 mg/kg). Animals that received a control injection received 100 μl of PBS. In both cases, mice were briefly anesthetized (<30 s under 2.5% isoflurane), and injections were intra-peritoneal. Injections were always performed one hour prior to behavioral testing. Mice were assigned to CNO or control groups randomly, and all behavioral testing was performed in a blinded fashion.

Open-field analysis—To control for the potential for CNO induced effects on locomotion, mice were assayed post-injection in an open-field environment. Mice were randomly assigned to first receive an injection of saline or CNO (10 mg/kg), following injection practices identical to those previously described. One hour post-injection, mice were placed in a 31 cm × 26.5 cm rectangular environment, and their motion was videotaped for 5 minutes. 6 hours later mice received a second intra-peritoneal injection different from the injection they received in the first round, and were then placed once more in the rectangular environment. Animal motion was analyzed using BIOBSERVE Viewer 2.

Measures assessed include the time spent in the center of the rectangular zone (19 cm × 14.5 cm), and the average velocity of animal movement over the 5 minute period.

Measurement of histamine-induced itch with concurrent optogenetic stimulation and intrathecal agent administration

Mice used in this experiment were SOM-ChR2+ or mCherry+ mice. Mice were initially briefly anesthetized (<1 minute at 2.5% isoflurane), and received both an intradermal injection of histamine dichloride (20 μl, 400 μg) as well as an intrathecal injection of either PBS or the SST2R antagonist CYN-154806 (10 μl injection, 250 ng). Intrathecal injections were performed using a 30G syringe. Needle insertion was confirmed with a visible tail flick.

Measurement of sensorimotor coordination

Measurement of adhesion tape removal latency was not performed in a blind manner, as it was impossible to apply the sticky tape without observing whether or not a mouse was cannulated. Mice were briefly restrained and a 1 f piece of sticky tape was applied to the dorsal surface of the right hind paw. The amount of time until the mouse began trying to remove the tape was determined using a stopwatch.

Spontaneous response scoring

To judge whether a mouse responded to spinal cord illumination in a blinded fashion, we developed a scoring method whereby mice were assigned a score of zero, one, or two based on an observer's certainty that the mouse responded to the onset of illumination. A score of two corresponded to absolute certainty of a behavioral response, and a score of zero corresponded to no behavioral response. A score of one was given to mice who seemed to attend the stimulus, but who did not display a clear, canonical response.

Gait analysis

The Cat-Walk analysis and the required training protocol has been described elsewhere (Deumens et al., 2007; Hamers et al., 2001). For our studies, mice were trained and tested on the same day. The mouse home cage was placed at the end of the walkway as a reward, and animals were trained with at least three runs across the walkway before testing. Trials were included if the following parameters were met: minimum run duration: 0.5 s, maximum run duration: 15 s, minimum number of compliant runs to acquire: three, maximum allowed speed variation: 60%. We averaged across three compliant trials for each mouse.

To analyze these data, contralateral paws were used as internal controls; as all implantations were bilateral, any damage would present itself as a gait asymmetry. We analyzed stride length, swing time, swing speed, and stance time.

Computational modeling of light propagation

We adopted a simulation approach developed by Joshua Gordon (Stujenske et al., 2015), modifying the MATLAB scripts available in that work. Briefly, the simulation performs a Monte Carlo simulation of photons doing a random walk through tissue after realistically modelled emission from a fiber optic cannulae. Due to the prevalence of white matter tracts

in the spinal cord, we modified the stimulation parameters used by Stujenske, et al. (absorption, scattering, and anisotropy constants) to be those measured from ex-vivo human white matter (Yaroslavsky et al., 2002). This is an upper bound on the amount of scattering expected in real spinal cord tissue, and therefore our estimate of light penetration depth is a conservative one.

Immunohistochemistry, imaging, and quantification of transduction

Mice were deeply anesthetized, and then transcardially perfused with 10 ml of 1× PBS and 10 ml of 4% PFA. Spinal cords were dissected, fixed overnight in 4% PFA, and then cryopreserved in 30% sucrose. After being frozen in Tissue-Tek O.C.T, spinal cord sections were cut, either transversely, or longitudinally, at 20–40 μm on a cryostat (Leica CM3050S) and mounted on slides. After rinsing, slides were blocked in 0.3% Triton X-100, 2% Normal Donkey Serum (NDS) in PBS for 1 hour. Samples were incubated at room temperature overnight with primary antibodies (0.3% Triton X-100, 5% NDS, in PBS). Slides were then rinsed in PBS, and then incubated at room temperature for 2 hours with secondary antibodies in PBS. Slides were then rinsed, and coverslipped using PVA DABCO. Primary antibodies used were: Rabbit anti-GFAP (1:1000, #7260, Abcam), Rabbit anti-iba1 (1:400, #019-19741, Wako), Rabbit anti-PKCγ (1:400, #sc-211, Santa Cruz Biotechnology), Guinea Pig anti-NK1R (1:500, AB15810, EMD Millipore), Rabbit anti-SST2R (1:500, ab134152, Abcam), and Rabbit anti-cFos (1:500, ab7963, Abcam). Secondary antibodies used were: Donkey anti-Rabbit Cy5 (1:500, #711-175-152, Jackson Laboratories), Donkey anti-Rabbit Cy3 (1:500, #711-165-152, Jackson Laboratories), and Donkey anti-Guinea Pig Cy5 (1:500, #706-175-148, Jackson Laboratories).

Slides were imaged using a Leica TCS SP5 confocal scanning laser microscope, using 10×, 20×, 40×, and 63× objectives. Images were processed using Fiji, and image brightness and contrast adjusted if necessary. All such adjustments were applied uniformly to the entire image. For spinal cord PKCγ overlap experiments, 1–3 sections per mouse were analyzed from 3 mice expressing ChR2-eYFP, and 3 mice expressing hM4D-mCherry.

Supplementary Material

Refer to Web version on PubMed Central for supplementary material.

Acknowledgments

We thank the Stanford Neuroscience Gene Vector and Virus Core, the Stanford Behavioral and Functional Neuroscience Laboratory as well as members of the Deisseroth, Scherrer, and Delp labs for insightful discussions and help with experiments. This study was supported by the U.S. National Institutes of Health (NINDS R01-NS080954), and the Stanford Bio-X NeuroVentures program. A.J.C was supported by a Texas Instruments Stanford Graduate Fellowship, S.M.I. was supported by a Howard Hughes Medical Institute International Student Research Fellowship, and by the Siebel Scholars Foundation. G.S. was supported by grants from NIH (DA031777), the Rita Allen Foundation and the American Pain Society.

References

Adamantidis A, Arber S, Bains JS, Bamberg E, Bonci A, Buzsáki G, Cardin JA, Costa RM, Dan Y, Goda Y, Graybiel AM, Häusser M, Hegemann P, Huguenard JR, Insel TR, Janak PH, Johnston D, Josselyn SA, Koch C, Kreitzer AC, Lüscher C, Malenka RC, Miesenböck G, Nagel G, Roska B,

Schnitzer MJ, Shenoy KV, Soltesz I, Sternson SM, Tsien RW, Tsien RY, Turrigiano GG, Tye KM, Wilson RI. Optogenetics: 10 years after ChR2 in neurons-views from the community. Nat Neurosci. 2015; 18:1202–12. DOI: 10.1038/nn.4106 [PubMed: 26308981]

Alilain WJ, Li X, Horn KP, Dhingra R, Dick TE, Herlitze S, Silver J. Light-induced rescue of breathing after spinal cord injury. J Neurosci. 2008; 28:11862–70. DOI: 10.1523/JNEUROSCI.3378-08.2008 [PubMed: 19005051]

Armbruster BN, Li X, Pausch MH, Herlitze S, Roth BL. Evolving the lock to fit the key to create a family of G protein-coupled receptors potently activated by an inert ligand. Proc Natl Acad Sci U S A. 2007; 104:5163–8. DOI: 10.1073/pnas.0700293104 [PubMed: 17360345]

Bardoni R, Tawfik VL, Wang D, François A, Solorzano C, Shuster SA, Choudhury P, Betelli C, Cassidy C, Smith K, de Nooij JC, Mennicken F, O'Donnell D, Kieffer BL, Woodbury CJ, Basbaum AI, MacDermott AB, Scherrer G. Delta Opioid Receptors Presynaptically Regulate Cutaneous Mechanosensory Neuron Input to the Spinal Cord Dorsal Horn. Neuron. 2014; 81:1443.doi: 10.1016/j.neuron.2014.03.006

Bonin RP, Wang F, Desrochers-Couture M, Gasecka A, Boulanger ME, Cote DC, De Koninck Y. Epidural optogenetics for controlled analgesia. Mol Pain. 2016; 12:1744806916629051.doi: 10.1177/1744806916629051 [PubMed: 27030718]

Bourane S, Duan B, Koch SC, Dalet A, Britz O, Garcia-Campmany L, Kim E, Cheng L, Ghosh A, Ma Q, Goulding M. Gate control of mechanical itch by a subpopulation of spinal cord interneurons. Science (80-). 2015; 350:550–554. DOI: 10.1126/science.aac8653

Boyden ES. Optogenetics and the future of neuroscience. Nat Neurosci. 2015; 18:1200–1201. DOI: 10.1038/nn.4094 [PubMed: 26308980]

Canales A, Jia X, Froriep UP, Koppes RA, Tringides CM, Selvidge J, Lu C, Hou C, Wei L, Fink Y, Anikeeva P. Multifunctional fibers for simultaneous optical, electrical and chemical interrogation of neural circuits in vivo. Nat Biotechnol. 2015; 33:277–284. DOI: 10.1038/nbt.3093 [PubMed: 25599177]

Carr FB, Zachariou V. Nociception and pain: lessons from optogenetics. Front Behav Neurosci. 2014; 8:69.doi: 10.3389/fnbeh.2014.00069 [PubMed: 24723861]

Chaplan SR, Bach FW, Pogrel JW, Chung JM, Yaksh TL. Quantitative assessment of tactile allodynia in the rat paw. J Neurosci Methods. 1994; 53:55–63. [PubMed: 7990513]

Copits BA, Pullen MY, Gereau RW. Spotlight on pain: optogenetic approaches for interrogating somatosensory circuits. Pain. 2016; doi: 10.1097/j.pain.0000000000000620

Cunningham CL, Gremel CM, Groblewski PA. Drug-induced conditioned place preference and aversion in mice. Nat Protoc. 2006; 1:1662–70. DOI: 10.1038/nprot.2006.279 [PubMed: 17487149]

Deisseroth K. Optogenetics: 10 years of microbial opsins in neuroscience. Nat Neurosci. 2015; 18:1213–1225. DOI: 10.1038/nn.4091 [PubMed: 26308982]

Deumens R, Jaken RJP, Marcus MAE, Joosten EAJ. The CatWalk gait analysis in assessment of both dynamic and static gait changes after adult rat sciatic nerve resection. J Neurosci Methods. 2007; 164:120–130. DOI: 10.1016/j.jneumeth.2007.04.009 [PubMed: 17532474]

Dougherty KJ, Zagoraiou L, Satoh D, Rozani I, Doobar S, Arber S, Jessell TM, Kiehn O. Locomotor rhythm generation linked to the output of spinal shox2 excitatory interneurons. Neuron. 2013; 80:920–33. DOI: 10.1016/j.neuron.2013.08.015 [PubMed: 24267650]

Duan B, Cheng L, Bourane S, Britz O, Padilla C, Garcia-Campmany L, Krashes M, Knowlton W, Velasquez T, Ren X, Ross SE, Lowell BB, Wang Y, Goulding M, Ma Q. Identification of Spinal Circuits Transmitting and Gating Mechanical Pain. Cell. 2014; 159:1417–1432. DOI: 10.1016/j.cell.2014.11.003 [PubMed: 25467445]

English JG, Roth BL. Chemogenetics-A Transformational and Translational Platform. JAMA Neurol. 2015; 72:1361–6. DOI: 10.1001/jamaneurol.2015.1921 [PubMed: 26409113]

Foster E, Wildner H, Tudeau L, Haueter S, Ralvenius WT, Jegen M, Johannssen H, Hösli L, Haenraets K, Ghanem A, Conzelmann KK, Bösl M, Zeilhofer HU. Targeted ablation, silencing, and activation establish glycinergic dorsal horn neurons as key components of a spinal gate for pain and itch. Neuron. 2015; 85:1289–304. DOI: 10.1016/j.neuron.2015.02.028 [PubMed: 25789756]

Hägglund M, Borgius L, Dougherty KJ, Kiehn O. Activation of groups of excitatory neurons in the mammalian spinal cord or hindbrain evokes locomotion. Nat Neurosci. 2010; 13:246–52. DOI: 10.1038/nn.2482 [PubMed: 20081850]

Hägglund M, Dougherty KJ, Borgius L, Itohara S, Iwasato T, Kiehn O. Optogenetic dissection reveals multiple rhythmogenic modules underlying locomotion. Proc Natl Acad Sci U S A. 2013; 110:11589–94. DOI: 10.1073/pnas.1304365110 [PubMed: 23798384]

Hamers FP, Lankhorst AJ, van Laar TJ, Veldhuis WB, Gispen WH. Automated quantitative gait analysis during overground locomotion in the rat: its application to spinal cord contusion and transection injuries. J Neurotrauma. 2001; 18:187–201. DOI: 10.1089/08977150150502613 [PubMed: 11229711]

Ho JS, Tanabe Y, Iyer SM, Christensen AJ, Grosenick L, Deisseroth K, Delp SL, Poon ASY. Self-Tracking Energy Transfer for Neural Stimulation in Untethered Mice. Phys Rev Appl. 2015; 4:024001.doi: 10.1103/PhysRevApplied.4.024001

Iyer SM, Montgomery KL, Towne C, Lee SY, Ramakrishnan C, Deisseroth K, Delp SL. Virally mediated optogenetic excitation and inhibition of pain in freely moving nontransgenic mice. Nat Biotechnol. 2014; 32:274–278. DOI: 10.1038/nbt.2834 [PubMed: 24531797]

Iyer SM, Vesuna S, Ramakrishnan C, Huynh K, Young S, Berndt A, Lee SY, Gorini CJ, Deisseroth K, Delp SL. Optogenetic and chemogenetic strategies for sustained inhibition of pain. Sci Rep. 2016; 6:30570.doi: 10.1038/srep30570 [PubMed: 27484850]

Kardon AP, Polgár E, Hachisuka J, Snyder LM, Cameron D, Savage S, Cai X, Karnup S, Fan CR, Hemenway GM, Bernard CS, Schwartz ES, Nagase H, Schwarzer C, Watanabe M, Furuta T, Kaneko T, Koerber HR, Todd AJ, Ross SE. Dynorphin acts as a neuromodulator to inhibit itch in the dorsal horn of the spinal cord. Neuron. 2014; 82:573–86. DOI: 10.1016/j.neuron.2014.02.046 [PubMed: 24726382]

Malmberg AB, Chen C, Tonegawa S, Basbaum AI. Preserved acute pain and reduced neuropathic pain in mice lacking PKCgamma. Science. 1997; 278:279–83. DOI: 10.1126/science.278.5336.279 [PubMed: 9323205]

Melzack R, Wall PD. Pain mechanisms: a new theory. Science. 1965; 150:971–9. [PubMed: 5320816]

Montgomery KL, Iyer SM, Christensen AJ, Deisseroth K, Delp SL. Beyond the brain: Optogenetic control in the spinal cord and peripheral nervous system. Sci Transl Med. 2016; 8:337rv5.doi: 10.1126/scitranslmed.aad7577

Montgomery KL, Yeh AJ, Ho JS, Tsao V, Mohan Iyer S, Grosenick L, Ferenczi EA, Tanabe Y, Deisseroth K, Delp SL, Poon ASY. Wirelessly powered, fully internal optogenetics for brain, spinal and peripheral circuits in mice. Nat Methods. 2015; 12:969–974. DOI: 10.1038/nmeth.3536 [PubMed: 26280330]

Nishida K, Matsumura S, Taniguchi W, Uta D, Furue H, Ito S. Three-dimensional distribution of sensory stimulation-evoked neuronal activity of spinal dorsal horn neurons analyzed by in vivo calcium imaging. PLoS One. 2014; 9:e103321.doi: 10.1371/journal.pone.0103321 [PubMed: 25100083]

Otchy TM, Wolff SBE, Rhee JY, Pehlevan C, Kawai R, Kempf A, Gobes SMH, Ölveczky BP. Acute off-target effects of neural circuit manipulations. Nature. 2015; 528:358–363. DOI: 10.1038/nature16442 [PubMed: 26649821]

Park, SIl, Brenner, DS., Shin, G., Morgan, CD., Copits, BA., Chung, HU., Pullen, MY., Noh, KN., Davidson, S., Oh, SJ., Yoon, J., Jang, KI., Samineni, VK., Norman, M., Grajales-Reyes, JG., Vogt, SK., Sundaram, SS., Wilson, KM., Ha, JS., Xu, R., Pan, T., Kim, TI., Huang, Y., Montana, MC., Golden, JP., Bruchas, MR., Gereau, RW., Rogers, JA. Soft, stretchable, fully implantable miniaturized optoelectronic systems for wireless optogenetics. Nat Biotechnol. 2015; 33:1280–1286. DOI: 10.1038/nbt.3415 [PubMed: 26551059]

Petitjean H, Pawlowski SA, Fraine SL, Sharif B, Hamad D, Fatima T, Berg J, Brown CM, Jan LY, Ribeiro-da-Silva A, Braz JM, Basbaum AI, Sharif-Naeini R. Dorsal Horn Parvalbumin Neurons Are Gate-Keepers of Touch-Evoked Pain after Nerve Injury. Cell Rep. 2015; 13:1246–1257. DOI: 10.1016/j.celrep.2015.09.080 [PubMed: 26527000]

Snyder, LM., Ross, SE. Pharmacology of Itch, Handbook of experimental pharmacology, Handbook of Experimental Pharmacology. Springer Berlin Heidelberg; Berlin, Heidelberg: 2015.

Stujenske JM, Spellman T, Gordon JA. Modeling the Spatiotemporal Dynamics of Light and Heat Propagation for In Vivo Optogenetics. Cell Rep. 2015; 12:525–34. DOI: 10.1016/j.celrep.2015.06.036 [PubMed: 26166563]

Talpalar AE, Endo T, Löw P, Borgius L, Hägglund M, Dougherty KJ, Ryge J, Hnasko TS, Kiehn O. Identification of minimal neuronal networks involved in flexor-extensor alternation in the mammalian spinal cord. Neuron. 2011; 71:1071–84. DOI: 10.1016/j.neuron.2011.07.011 [PubMed: 21943604]

Todd AJ. Anatomy of primary afferents and projection neurones in the rat spinal dorsal horn with particular emphasis on substance P and the neurokinin 1 receptor. Exp Physiol. 2002; 87:245–9. [PubMed: 11856970]

Urban DJ, Roth BL. DREADDs (Designer Receptors Exclusively Activated by Designer Drugs): Chemogenetic Tools with Therapeutic Utility. Annu Rev Pharmacol Toxicol. 2015; 55:399–417. DOI: 10.1146/annurev-pharmtox-010814-124803 [PubMed: 25292433]

Wang H, Siddharthan V, Kesler KK, Hall JO, Motter NE, Julander JG, Morrey JD. Fatal neurological respiratory insufficiency is common among viral encephalitides. J Infect Dis. 2013; 208:573–83. DOI: 10.1093/infdis/jit186 [PubMed: 23641019]

Wang H, Zylka MJ. Mrgprd-expressing polymodal nociceptive neurons innervate most known classes of substantia gelatinosa neurons. J Neurosci Off J Soc Neurosci. 2009; 29:13202–9. DOI: 10.1523/JNEUROSCI.3248-09.2009

Yang K, Ma R, Wang Q, Jiang P, Li YQ. Optoactivation of parvalbumin neurons in the spinal dorsal horn evokes GABA release that is regulated by presynaptic GABAB receptors. Neurosci Lett. 2015; 594:55–9. DOI: 10.1016/j.neulet.2015.03.050 [PubMed: 25817363]

Yaroslavsky AN, Schulze PC, Yaroslavsky IV, Schober R, Ulrich F, Schwarzmaier HJ. Optical properties of selected native and coagulated human brain tissues in vitro in the visible and near infrared spectral range. Phys Med Biol. 2002; 47:305.doi: 10.1088/0031-9155/47/12/305 [PubMed: 11837619]

Yizhar O, Fenno LE, Davidson TJ, Mogri M, Deisseroth K. Optogenetics in neural systems. Neuron. 2011; 71:9–34. DOI: 10.1016/j.neuron.2011.06.004 [PubMed: 21745635]

Zhang Y, Yue J, Ai M, Ji Z, Liu Z, Cao X, Li L. Channelrhodopsin-2-expressed dorsal root ganglion neurons activates calcium channel currents and increases action potential in spinal cord. Spine (Phila Pa 1976). 2014; 39:E865–9. DOI: 10.1097/BRS.0000000000000373 [PubMed: 25171072]

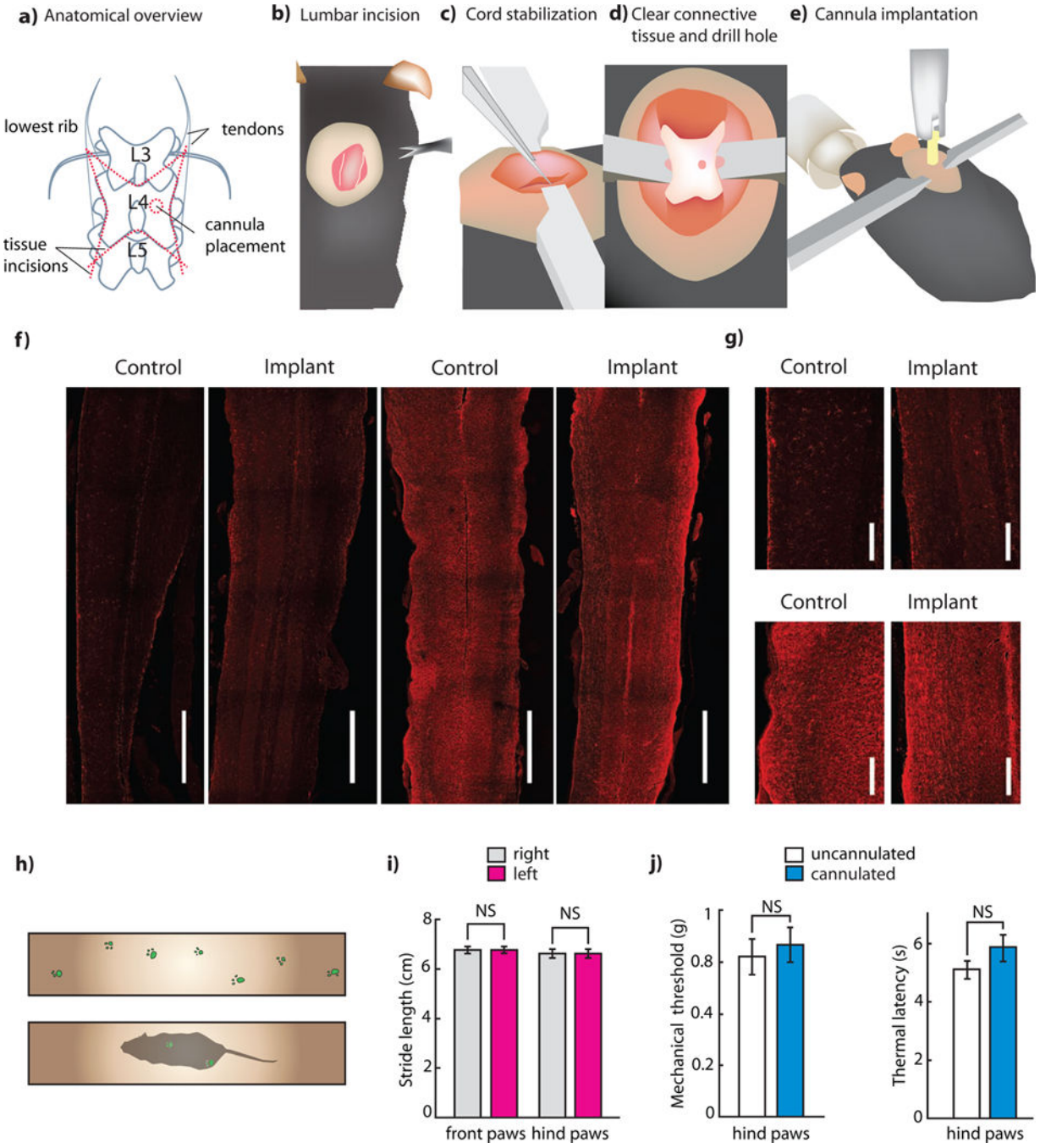

Figure 1. Implantation of fiber optic ferrules for light delivery to the spinal cord

(a) Schematic showing relevant surgical landmarks. **(b)–(e)** Schematics showing process of implantation of fiber optic cannula. **(f)** Representative longitudinal spinal cord sections from control and implanted mice stained for astrocyte (GFAP) or microglia activations (Iba1). (2 sections each from $n = 3$ experimental and $n = 3$ control were analyzed) Scale bar: 1 mm. **(g)** Close up of implantation region for Iba1 and GFAP stained longitudinal sections. Scale bar: 250 μm **(h)** Schematic showing catwalk and representative gait trace of cannulated mouse. **(i)** Stride length of ipsilateral vs. contralateral paws of implanted mice ($n = 5$. $P = 0.397$). **(j)**

Mechanical withdrawal thresholds of cannulated and uncannulated mice, as measured on the von Frey test (n = 10 implanted, 10 wild type. P = 0.528). Thermal withdrawal latencies of cannulated and uncannulated mice, as measured on the Hargreaves test (n = 10 implanted, 10 wild type. P = 0.47). All group data is shown as mean ± s.e.m.

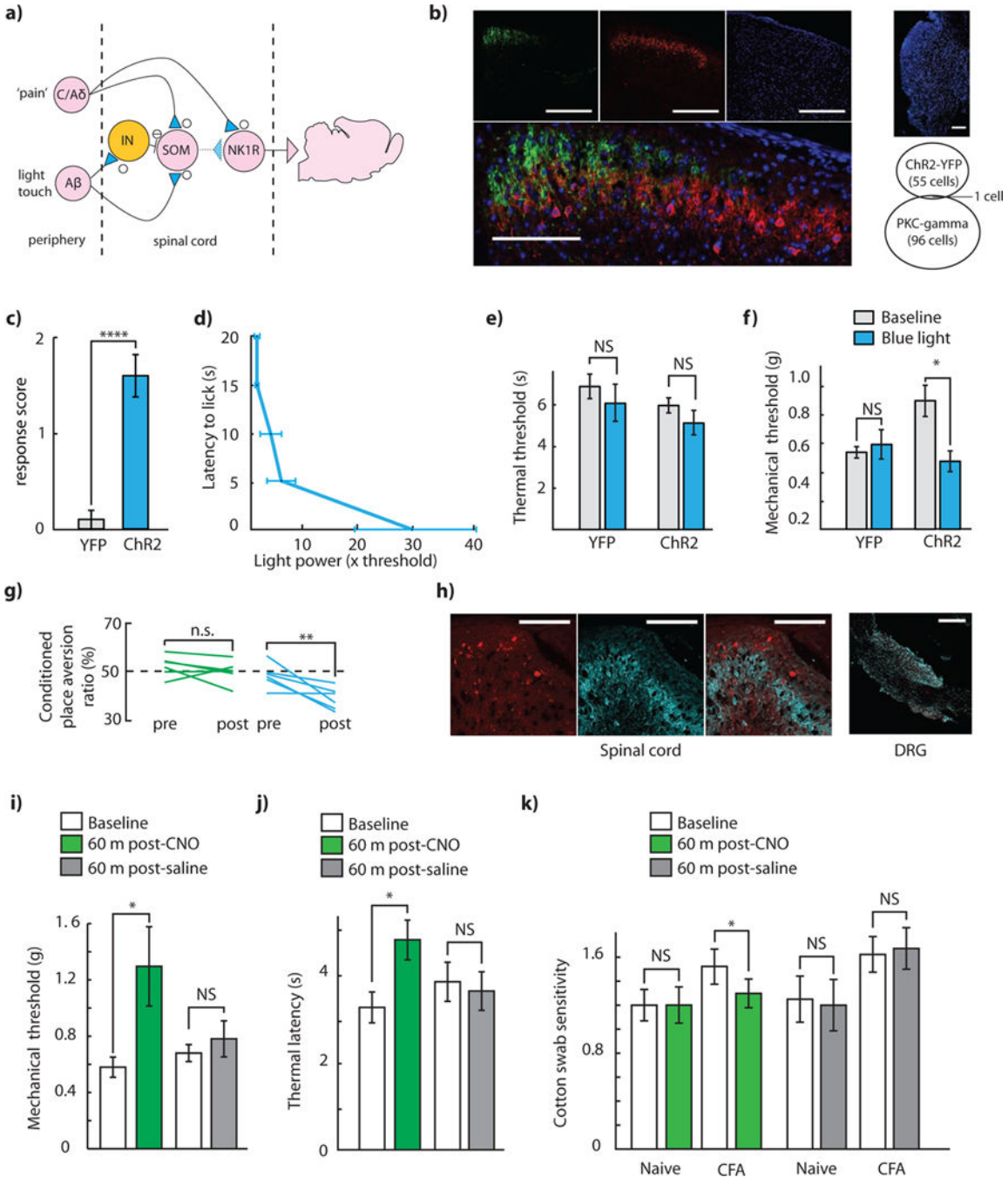

Figure 2. Optogenetic and chemogenetic modulation of somatostatin interneurons

(a) Diagram of primary afferent to brain circuit containing somatostatin interneurons. Hypothesized and/or polysynaptic connection shown in dotted lines. **(b)** Histology showing somatostatin expression (sections from $n = 3$ mice were examined for quantification). Scale bar: 250 μm, inset: 100 μm. **(c)** Spontaneous response score of YFP mice compared to ChR2 mice in somatostatin interneurons ($n = 5$ ChR2, 5 YFP, $P = 4\times10^{-4}$). **(d)** Latency to lick response of somatostatin mice vs. threshold light power ($n = 7$ mice, each normalized to their individual threshold, binned in 5 second intervals, and then averaged across mice). **(e)**

Thermal withdrawal latency during 'subthreshold' blue light illumination of YFP mice and ChR2 mice (n = 5 ChR2, 5 YFP. P = 0.1 YFP, P = 0.21 control). **(f)** Mechanical withdrawal thresholds of YFP and ChR2 mice at baseline and during subthreshold blue light illumination (n = 5 ChR2, 5 YFP. P = 0.421 YFP, P = 0.0173 ChR2). **(g)** Conditioned place aversion (CPA) ratios, calculated as the ratio of the percentage of time spent in the stimulation chamber on initial (pre-test) day, and after three days of conditioning (n = 6 ChR2, 6 YFP. ChR2: P = 0.006, control: P = 0.208). **(h)** Histology indicating robust expression of hM4D in the spinal cord dorsal horn following intraspinal injection of AAV5::hM4D, indicating expressing in lamina II that is non-overlapping with PKCγ. Top row, transverse spinal cord section: hM4D-mCherry (red), PKCγ (cyan), overlap. Scale bar: 100 μm. Bottom row, dorsal root ganglion section: hM4D-mCherry (red), DAPI (cyan). Scale bar: 250 μm. **(i)** Mechanical withdrawal thresholds following injection of CNO or saline in SOM-hM4D+ mice (n = 8 post-CNO, n = 8 post-saline, P (post-CNO) = 0.013, P (post-saline) = 0.52). **(j)** Thermal withdrawal latency following injection of CNO or saline in SOM-hM4D+ mice (n = 7 post-CNO, n = 7 post-saline, P (post-CNO) = 0.047, P (post-saline) = 0.66). **(k)** Cotton swab sensitivity following injection of CNO or saline in SOM-hM4D+ mice before and after intraplantar CFA. (Pre-CFA: n = 8 post-CNO, n = 8 post-saline. Post-CFA: n = 8 post-CNO, n = 8 post-saline. Pre-CFA: P (post-CNO) = 1, P (post-saline) = 0.84. Post-CFA: P (post-CNO) = 0.015, P (post-saline) = 0.60). All group data is shown as mean ± s.e.m.

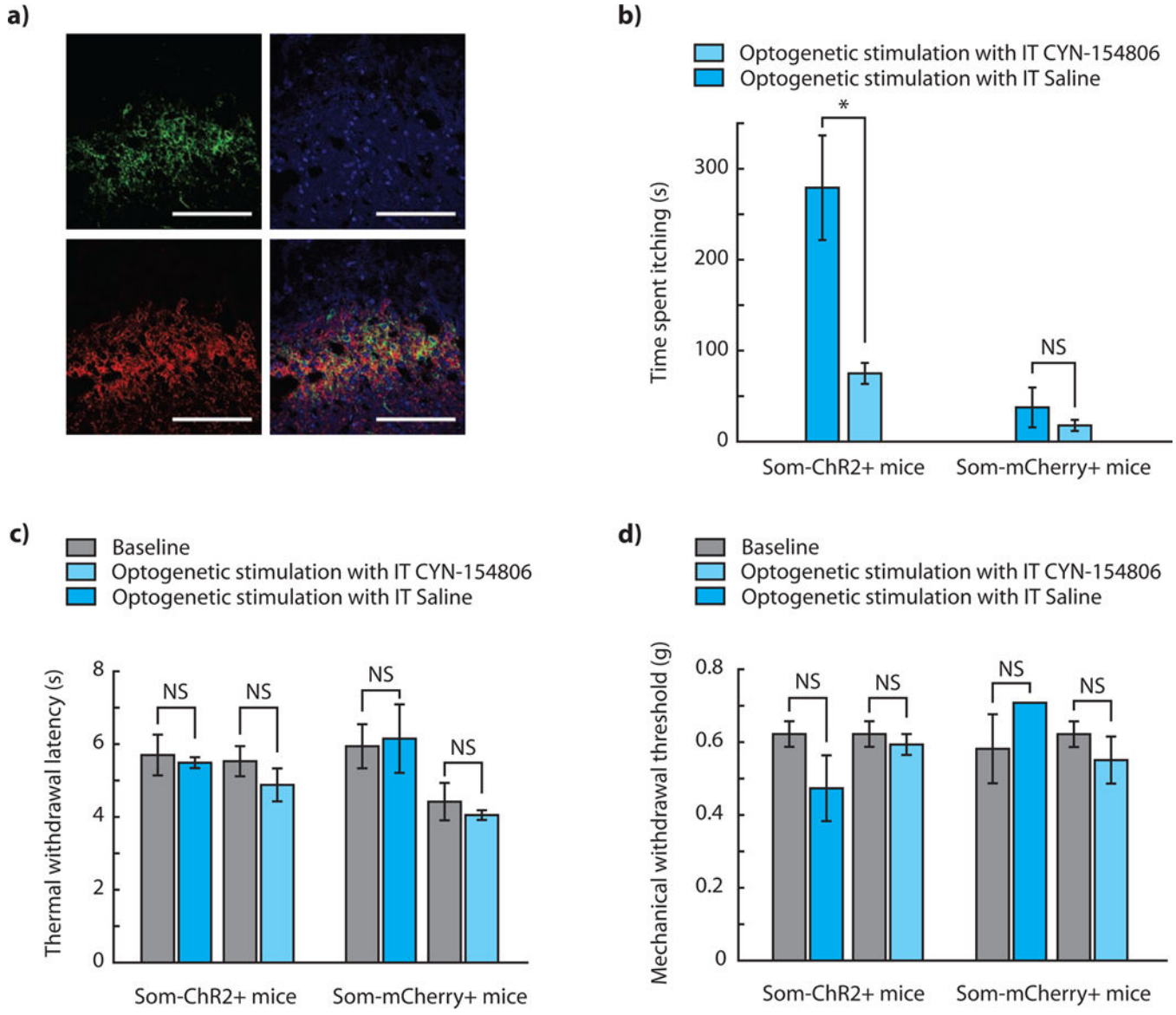

Figure 3. Temporally sparse optogenetic stimulation of somatostatin interneurons modulates pruritoception

(a) Histology indicating significant spatial proximity between ChR2+ neurons and SST2R immunoreactivity in SOM-ChR2+ mice. Clockwise from top-left: green: ChR2-eYFP, blue: DAPI, red: SST2R immunoreactivity, overlay. Scale bar: 100 μm. **(b)** Time spent itching during sparse optogenetic stimulation in SOM-ChR2 and SOM-mCherry mice, with concurrent intrathecal CYN-154806 or intrathecal saline. (n = 6 SOM-ChR2+ mice, n = 5 SOM-mCherry+ mice, P (SOM-ChR2) = 0.028, P (SOM-mCherry) = 0.47). **(c)** Thermal withdrawal latency during sparse optogenetic stimulation in SOM-ChR2 and SOM-mCherry mice, with concurrent intrathecal CYN-154806 or intrathecal saline (n = 5 mice in all conditions, P (SOM-ChR2 + CYN-154806) = 0.042, P (SOM-ChR2 + saline) = 0.77, P (SOM-mCherry + CYN-154806) = 0.54, P (SOM-mCherry + saline) = 0.78)). **(d)** Mechanical withdrawal thresholds during sparse optogenetic stimulation in SOM-ChR2 and

SOM-mCherry mice, with concurrent intrathecal CYN-154806 or intrathecal saline ($n = 5$ mice in all conditions, P(SOM-ChR2 + CYN-154806) = 0.37, P(SOM-ChR2 + saline) = 0.10, P(SOM-mCherry + CYN-154806) = 0.22, P(SOM-mCherry + saline) = 0.25). All group data is shown as mean ± s.e.m.

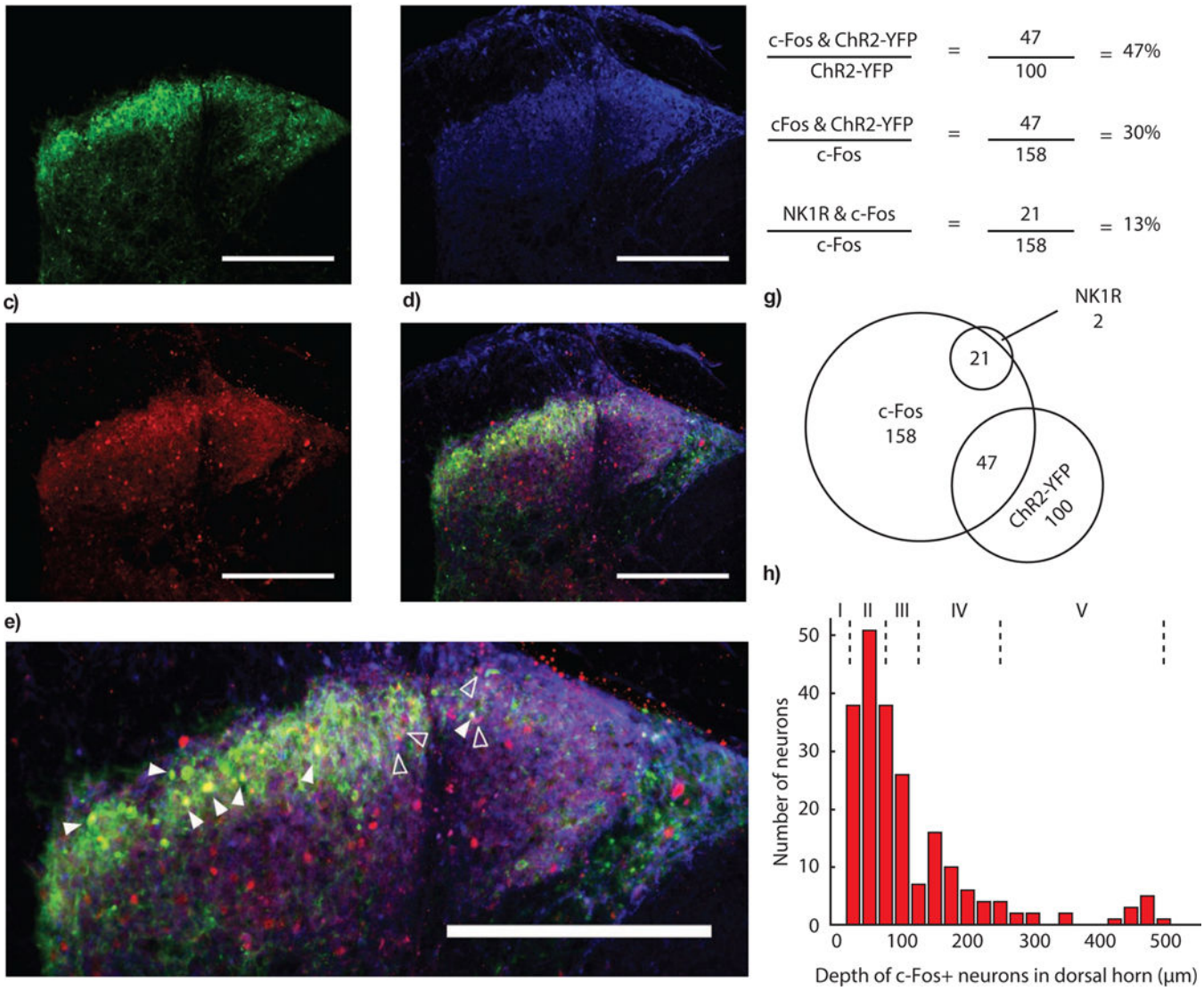

Figure 4. c-Fos activation in the dorsal horn after stimulation of somatostatin interneurons

(a) ChR2-eYFP fluorescence in the dorsal horn after intraspinal injection of AAVDJ:ef1a:DIO:ChR2-eYFP in SOM-IRES-Cre mice. **(b)** Immunostaining for NK1R in the dorsal horn of the spinal cord. **(c)** c-Fos expression in the dorsal horn after expression of somatostatin in the spinal cord. **(d)** Merge of c-Fos, ChR2-eYFP, and NK1R channels. Scale bar (a–d): 250 μm. **(e)** Examples of overlap of c-Fos and YFP (closed arrows), or c-Fos and NK1R (open arrows). Scale bar: 250 μm. **(f)** Quantification of overlap of c-Fos, YFP and NK1R expression. Note: 56 ± 8 % of ChR2+ cells are also c-Fos+, The ChR2+/c-Fos+ to ChR2−/c-Fos+ ratio is 2.55 ± 0.44. **(g)** Visualization of overlap. **(h)** Quantification of depth of c-Fos expressing neurons in the dorsal horn. Lamina depths are denoted with dotted lines and roman numerals.